Mon. Not. R. Astron. Soc. **000**, 000–000 (0000) Printed 5 August 2002 (MN LaTeX style file v1.4)

Understanding the Results of Galaxy-Galaxy Lensing using Galaxy-Mass Correlation in Numerical Simulations

XiaoHu Yang[1,2,3], H. J. Mo[1], Guinevere Kauffmann[1], YaoQuan Chu[2,3]
[1] *Max-Planck-Institut für Astrophysik Karl-Schwarzschild-Strasse 1, 85748 Garching, Germany*
[2] *Center for Astrophysics, University of Science and Technology of China, Hefei, Anhui 230026, China*
[3] *National Astronomical Observatories, Chinese Academy of Science, Chao-Yang District, Beijing, 100012, China*

Accepted .... Received ....; in original form ....

ABSTRACT

McKay et al. (2002) have recently used measurements of weak galaxy-galaxy lensing in the Sloan Digital Sky Survey to estimate the cross correlation between galaxies and the projected dark matter density field. They derive a relation between aperture mass within a radius of $260\,h^{-1}$kpc, M_{260}, and lens galaxy luminosity, that does not depend on galaxy luminosity, type or environment. In this paper, we study the cross-correlation between galaxies and dark matter using galaxy catalogs constructed from a high-resolution N-body simulation of a ΛCDM Universe. We show that our simulations reproduce the McKay et al. results reasonably well. In the simulation, M_{260} is approximately equal to the halo virial mass for L_* galaxies. M_{260} overestimates the virial mass for fainter galaxies and underestimates it for brighter galaxies. We use the simulations to show that under certain circumstances the halo virial mass may be recovered by fitting an NFW profile to the projected galaxy-mass correlation function. If we apply our method to the observations, we find that L_* galaxies typically reside in halos of $\sim 2\times 10^{12}h^{-1}\mathrm{M}_\odot$, consistent with halo masses estimated from the observed Tully-Fisher relation. In the simulations, the halo virial mass scales with galaxy luminosity as $L^{1.5}$ for central galaxies in halos and for galaxies in low-density regions. For satellite galaxies, and for galaxies in high-density regions, there is no simple relation between galaxy luminosity and halo mass and care must be exercised when interpreting the lensing results.

Key words: dark matter - gravitational lensing - large-scale structure of the universe - galaxies: halos - methods: statistical

1 INTRODUCTION

In a recent study, McKay et al. (2002, herafter M2002) used the signal of galaxy-galaxy lensing detected in the Sloan Digital Sky Survey (SDSS) to infer the dark matter mass distribution around bright galaxies. What McKay et al. measured from the data was the shear field γ_+, inferred from the distorted images of background galaxies around lensing galaxies. From the theory of weak lensing (e.g. Schneider et al., 1999), the shear field is related to the surface mass density contrast $\Delta\Sigma_+$ as:

$$\gamma_+(R)\Sigma_{crit} = \overline{\Sigma}(\leq R) - \overline{\Sigma}(R) \equiv \Delta\Sigma_+\,, \qquad (1)$$

where $\overline{\Sigma}(\leq R)$ is the mean surface density within radius R, $\overline{\Sigma}(R)$ is the mean surface density at radius R, and $\Sigma_{\rm crit}$ is the critical density determined by the geometry of the lens-source system. Defined this way, $\Delta\Sigma_+$ is a measure of the cross correlation between the lens galaxies and the projected mass density. We will therefore refer $\Delta\Sigma_+$ as the galaxy-mass correlation function (GMCF).

The GMCF depends on the matter distribution around lens galaxies. The observed GMCF can therefore be used to infer the extent of dark haloes around galaxies (e.g. Hudson et al. 1998; Fischer et al. 2000; Smith et al. 2001; Wilson et al. 2001; Guzik & Seljak 2002). Using the SDSS data, McKay et al. (M2002) found that: (i) the shear field γ_+ could be measured with reasonable signal-to-noise out to a projected radius $\sim 1\,h^{-1}$Mpc; (ii) $\Delta\Sigma_+(R)$ could be fit by a power law, with the singular isothermal sphere an acceptable model for the distribution of dark matter around galaxies; (iii) the mass M_{260} (defined as the mass projected within an aperture of radius $260\,h^{-1}$kpc) inferred from the observed GMCF was strongly correlated with the luminosity of lens galaxies and in the redder photometric pass-bands, the galaxy luminosity was proportional to M_{260}, with a proportionality constant of order 100; (iv) the ratio of aperture mass to luminosity in the red photometric bands did not depend significantly on galaxy luminosity, type and environment.

Because current models of galaxy formation based on the cold dark matter (CDM) cosmogony predict the existence of extended dark haloes around galaxies, the results of M2002 provide important constraints on models of galaxy formation.

The observed GMCF cannot be interpreted simply in terms of individual halo profiles. There are three other factors that can affect it. First, the observed GMCF is an average of mass density fields around different galaxies. Second, the GMCF depends on how lens galaxies are distributed within dark haloes. Third, more than one halo can contribute to the projected density field around a given galaxy. These effects must be quantified in order to use the observed GMCF to infer the properties of galaxy haloes.

In this paper, we use a galaxy catalogue constructed from a high-resolution N-body simulation to understand the observed galaxy-galaxy lensing results. We first examine whether or not the simulation results agree with the observations. We then illustrate how the three effects mentioned above influence the GMCF. Finally, we discuss what kind of information about dark haloes it is possible to infer from the GMCF. The paper is organized as follows. In Section 2 we describe the simulation data. Calculations of the GMCFs for various samples are presented in Section 3. In Section 4, we investigate the relation between the masses derived from the GMCFs and the actual masses of dark haloes in the simulation. We then use these relations to estimate the halo masses of observed lens galaxies. Finally, in Section 5, we summarize and discuss our results.

2 THE SIMULATIONS

In this paper, we use the results of the GIF simulation of the ΛCDM model [with $(\Omega_0, \Lambda, \Gamma, \sigma_8) = (0.3, 0.7, 0.21, 0.90)$] carried out by Kauffmann et al. (1999) using codes from the Virgo Consortium (Jenkins et al., 1998; the data are publicly available *.) The simulation evolves 256^3 cold dark matter particles in a periodic cube of side length $141.3\mathrm{h}^{-1}$Mpc, with particle mass $1.4\times10^{10}h^{-1}M_\odot$, and with a force softening $\eta = 20\,h^{-1}$kpc. Dark haloes were selected from the simulation using a “friends-of-friends” (FOF) algorithm with a linking length of 0.2 times the mean inter-particle separation, and galaxy catalogues were constructed by populating dark haloes with galaxies according to a semi-analytic model of galaxy formation described in Kauffmann et al. (1999a). Model galaxies are assigned luminosities and morphological types according to their star formation histories and bulge-to-disk ratios. Previous investigations with these simulated catalogues demonstrated that the model is quite successful in matching the observed properties of the galaxy population, both at the present day and at high redshifts (Kauffmann et al., 1999a, b; Diaferio et al., 1999; 2001).

For this study, we use new publically available galaxy catalogues constructed from the GIF simulations giving predictions for the SDSS photometric bands. We present results only for the z-band. Calculations were also made for the r and i-bands, but the results are very similar. Fig. 1 shows the luminosity distribution of the model galaxies. Results are shown for ‘central galaxies’ (which are the brightest galaxies located at the centers of dark matter halos) and for ‘all galaxies’ (which include both central galaxies and satellites). As can be seen, the bright end of the luminosity function is dominated by central galaxies, while satellite galaxies dominate the faint end. Because of the mass resolution of the simulation, predictions for galaxies fainter than -19.5 mag are uncertain. Such galaxies are excluded from our analyses.

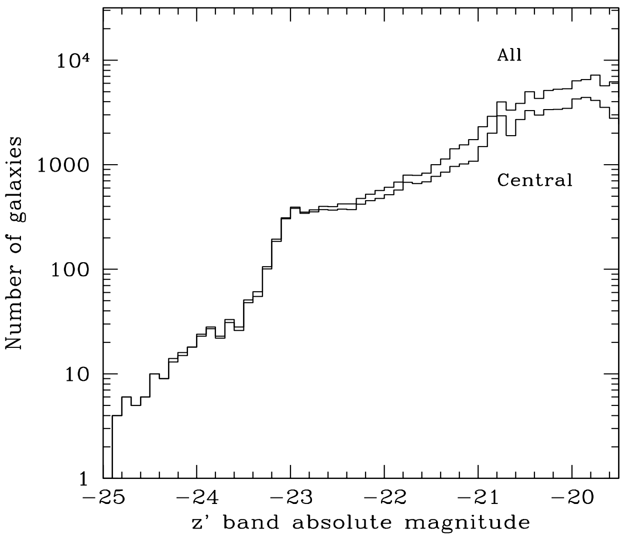

Figure 1. The distribution of GIF galaxies with respect to the z-band absolute magnitudes. Results are shown separately for central galaxies and all galaxies.

3 ANALYSES

3.1 The GMCF

As explained in Section 1, the observed shear fields around galaxies can be used to derive the cross-correlation between lens galaxies and the projected mass density field. In this paper, we calculate the GMCF directly from the mass and galaxy distributions in the simulations. We thus neglect all the uncertainties involved in reconstructing the mass-density field from the weak lensing observations.

We first project the positions of galaxies and dark matter particles onto a plane (chosen to be one surface of the simulation box). For each galaxy, we estimate the mean surface density contrast of dark matter within rings of different radii around the galaxy. The GMCF as a function of radius, $\Delta\Sigma_+(R)$, is obtained by averaging over a given sample of galaxies. Since by definition the background surface density is subtracted from $\Delta\Sigma_+(R)$, the derived GMCF is independent of the depth of the projection (here equal to the simulation box size), so long as this depth is much larger than the correlation length of dark matter.

The GMCF is estimated for two different kinds of lens galaxy samples:

* http://www.mpa-garching.mpg.de/Virgo/

- AG-sample, which contains all simulated galaxies in some luminosity range;
- CG-sample, which contains only central galaxies in some luminosity range.

To quantify the GMCF, we fit it by simple models. Following M2002, we first fit a GMCF with a power-law,

$$\Delta\Sigma_+ = A\ (R/1\,h^{-1}\mathrm{Mpc})^b\ h\mathrm{M}_\odot\mathrm{pc}^{-2}\,, \tag{2}$$

where A and b are the fitting parameters. Motivated by the fact that the density profiles of CDM haloes are well described by the NFW profile (Navarro, Frenk & White 1997), we also fit the GMCF by assuming the halo profile to have the form:

$$\rho(r) = \frac{\bar\delta\bar\rho}{(r/r_s)(1+r/r_s)^2}\,, \tag{3}$$

where $\bar\delta$ is a dimensionless density amplitude, r_s is a characteristic radius, and $\bar\rho$ is the mean background density. This profile is characterized by a virial radius r_{200} (defined to be the radius within which the average mass density is equal to $200\bar\rho$), and a dimensionless concentration parameter c (or a scale radius $r_s = r_{200}/c$). The amplitude $\bar\delta$ is related to c by

$$\bar\delta = \frac{200c^3}{3[\ln(1+c)+c/(1+c)]}\,. \tag{4}$$

The properties of the projected NFW profile are given in Appendix A.

We fit the GMCFs by equation (A6), with c and r_{200} as free parameters. Note that we are not fitting a single dark halo with the NFW profile (the GMCF is a superposition of different haloes), and so the values of c and r_{200} are not related to the concentration and radius of a single halo but the mean of many haloes. For both the power-law and NFW model, we restrict the fits to the range of radii between $0.05\,h^{-1}$Mpc and $1\,h^{-1}$Mpc.

In Fig. 2 we show the results of the GMCF for both AG and CG samples brighter than -19.5^m. These results are obtained using all simulated galaxies down to this magnitude limit and do not take into account the selection function in the observed data. Observational selection effects will be considered in subsection 3.3. As one can see from Fig. 2, the GMCFs for the AG and CG samples have rather different behaviour. For the CG sample, the GMCF is strongly peaked at small radii and tends towards zero at large radii. In this case, the GMCF profile is well-described by the simple models based on the projection of halo profiles. Not surprisingly, the NFW model gives a better fit than the power-law model. In contrast, the GMCF for the AG sample is less centrally peaked and tends towards a constant non-zero value at large radii. This occurs because many satellite galaxies are located at the outskirts of massive halos in the simulations. As demonstrated in Appendix B, the reduction in the amplitude of the GMCF on small scales is due to the separation between satellite galaxies and halo centers. The positive value at large radii is due to the extended distribution of mass in massive haloes. Note that the GMCF profile for the AG sample does not follow the simple models based the projections of halo density profiles.

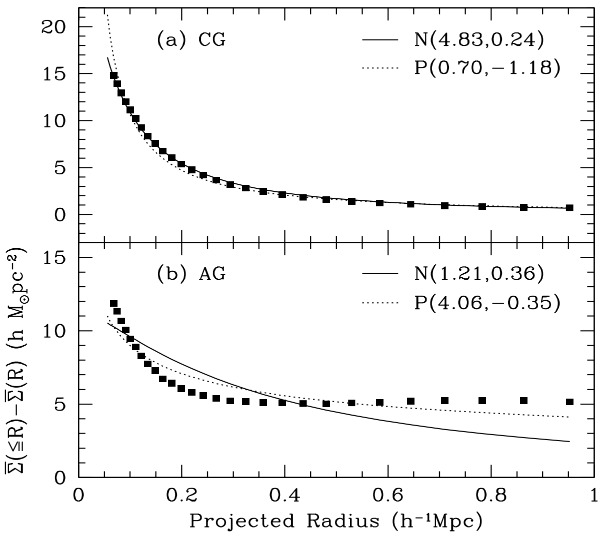

Figure 2. The GMCFs for the CG (squares in the upper panel) and AG (squares in the lower panel) samples constructed from the GIF galaxies with z'-magnitudes brighter than -19.5^m. The solid curve is the fit to the NFW model, with the fitting parameters c and r_{200} (in h^{-1}Mpc) given in N(c, r_{200}). The dotted curve is the fit to the power-law model, with the fitting parameters A and b given in P(A, b).

3.2 Dependence on galaxy properties

Fig. 3 and 4 show how the predicted GMCFs vary as a function of galaxy absolute magnitude. For bright magnitudes, most galaxies are central galaxies, and so both AG and CG samples give similar results. For galaxies fainter than about -21^m the AG and CG samples behave differently, because the contribution of satellite galaxies becomes important in the AG sample (for example, over one third of the galaxies with magnitudes in the range -21^m - -20^m are satellite galaxies, see Fig. 1). There is a clear trend that more luminous galaxies exhibit a stronger cross-correlation with the mass. This is expected, because luminous galaxies reside preferentially in more massive haloes. As we will show later, this result is reproduced quantitatively in the observational data.

As one can see, the GMCFs are well described by the NFW model for for central galaxies and for bright galaxies. The fit to the power-law model is not as good, but the difference is not big enough to be detectable in the current SDSS data. Note that for AG samples fainter than -21^m, the contamination by satellite galaxies becomes so important that no simple model can fit the GMCFs (see Fig. 4). These results show that the interpretation of the GMCF is much simpler for bright central galaxies.

In our simulation, the morphological classification of galaxies is made according to their B-band disk-to-bulge ratios. If $M_{B,\mathrm{bulge}} - M_{B,\mathrm{total}} < 1$ mag, the galaxy is classified as an early-type (elliptical or S0) galaxy; otherwise it is classified as a late-type (spiral) galaxy (see Kauffmann et al., 1999a for details). Due to the limited simulation resolution, morphological types are only assigned to galaxies with haloes containing more than ~ 100 particles. About 7850 (13500) galaxies in the CG (AG) sample are classified as el-

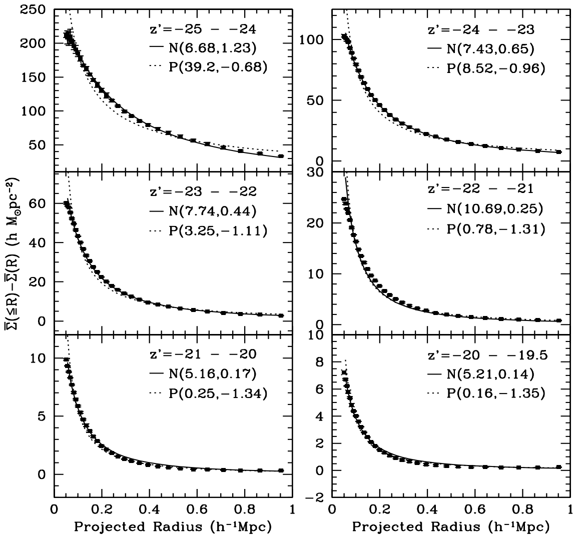

Figure 3. The GMCFs and the model fits for z-band galaxies in different luminosity ranges (CG samples). The best fit parameters are given as $\mathrm{N}(c, r_{200})$ for the NFW model and as $\mathrm{P}(A, b)$ for the power-law model. The errorbars are the scatter of the GMCFs obtained from three projections of the simulated density field.

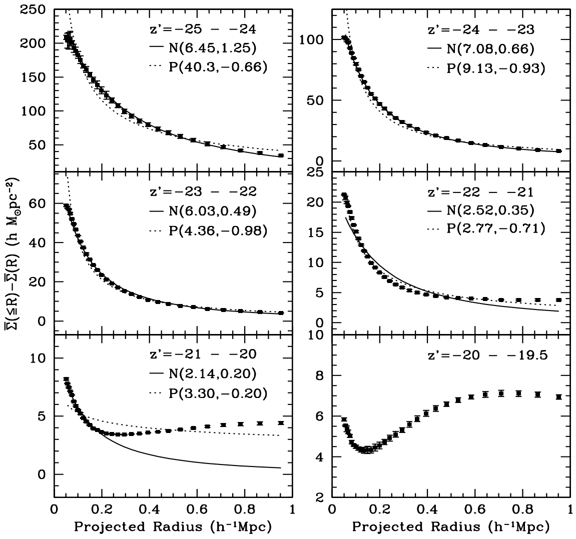

Figure 4. The same as Fig.3, but for AG samples. For galaxies fainter than -21^m, both power-law model and the NFW model fail to give an acceptable fit.

liptical galaxies, while about 53800 (80000) galaxies in the CG (AG) sample are classified as spiral galaxies. In Fig. 5 we compare the GMCFs of elliptical and spiral galaxies. Once again results are shown for all simulated galaxies without taking into account the observational selection function. As can be seen, the cross-corrrelation between early-type galaxies and dark matter is stronger than for late-type galaxies. In the simulation, these results come from the fact that early-type galaxies are preferentially located in massive haloes.

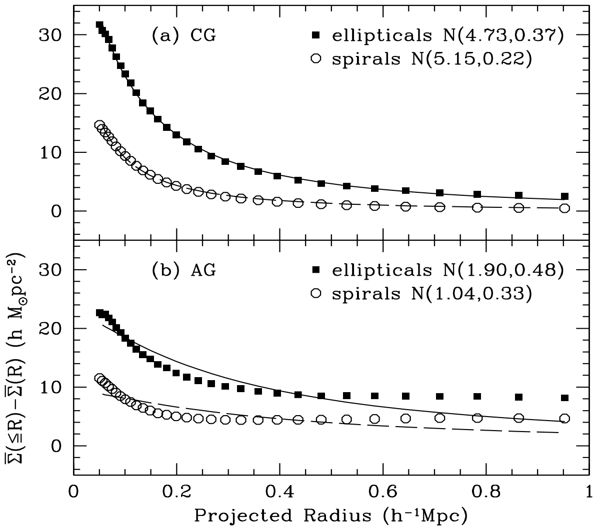

Figure 5. The GMCFs for elliptical (squares) and spiral (circles) galaxies. The upper panel is for CG samples, while the lower panel is for AG samples. Curves show the fits to the NFW model.

3.3 Incorporating observational selection effects

In order to compare model predictions with observational results, we should select galaxy samples in the same way as in the observations. The galaxy samples analyzed in M2002 are apparent – magnitude limited, and so fainter galaxies have smaller probability of being included. In this section, we select model galaxies according to the observed luminosity distribution of the lens galaxies (see figure 2 in M2002). There are some subtle effects associated with a magnitude - limited sample. For example, lens galaxies with different luminosities have different redshift distributions, and so their lensing strengths (i.e. the value of $\Sigma_{\rm crit}^{-1}$) are different. Furthermore, the angular radius corresponding to a given projected physical radius is larger at a smaller distance, and so the number of lensed sources ($N_{\rm source}$) within a given projected physical radius is larger for closer galaxies. In the analyses of M2002, lens galaxxies are weighted by $N_{sources} * \Sigma_{\rm crit}^{-2}$. To mimic this weighting, we use the curve of $\Sigma_{\rm crit}^{-1}$ given in M2002 and assume $N_{source} \propto r^{-2}$, where r is the angular-size distance to a lens. We calculate a mean weight for galaxies with a given luminosity by averaging $N_{\rm sources} * \Sigma_{\rm crit}^{-2}$ over the volume within the distance limit which corresponds to the luminosity in consideration, assuming that the distribution of such galaxies within the volume is uniform. We then assign to each model galaxy a mean weight corresponding to its luminosity. Note that the $N_{\rm source}$ used in M2002 takes into account other selection effects, such as the exclusion of lens galaxies around which the distributions of source galaxies are too asymmetric (see M2002 for details). Such selections may change the $N_{source} \propto r^{-2}$ relation but are not taken into account in our model.

Fig.6 shows the results of the GMCF for a sample of galaxies selected in the z-band. It turns out that most of the galaxies in the selected samples are luminous central galaxies and as a result, the GMCF can now be fitted reasonably well by the NFW model. Compared with the GMCFs derived

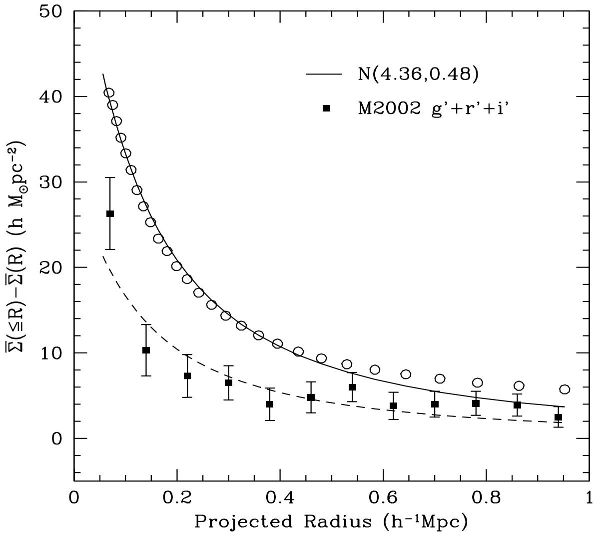

Figure 6. The GMCF and the model fit for the sample constructed with the SDSS selection function. The solid line is the fit to the NFW model, while the dashed line is half of the model fit. For comparison, the GMCFs derived by M2002 from the combined g'- r'- and i'-band images are shown as squares with errorbars. Note that M2002 only used the images in these three bands to measure the galaxy shapes. Although the predicted GMCF has the same shape as the observation, the predicted amplitude is too high by a factor of ~ 2.

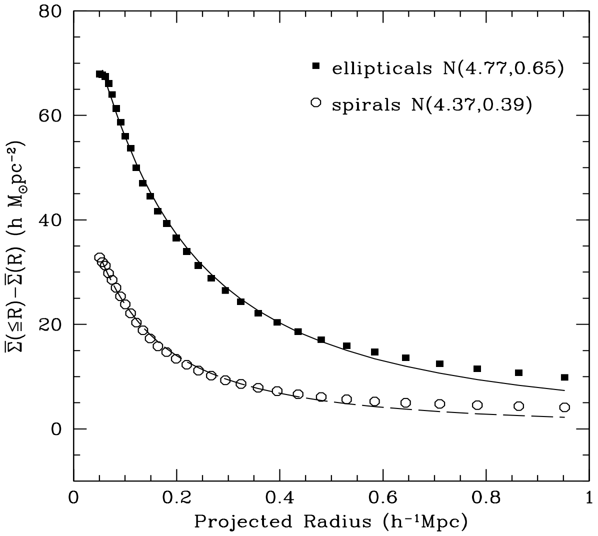

Figure 7. The GMCFs for elliptical (squares) and spiral (circles) samples with the SDSS selection function. Curves are fits to the NFW model.

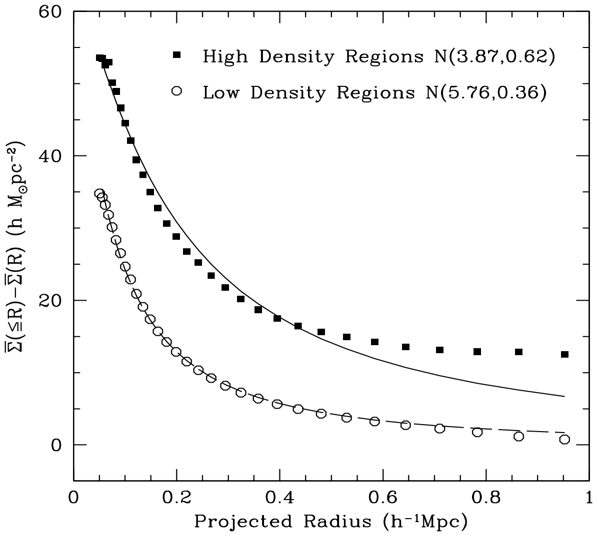

Figure 8. The GMCF for galaxies in high- (squares) and low-density (circles) regions, selected with the SDSS selection function. Curves are fits to the NFW model.

by M2002, our predicted GMCF has a similar shape but a higher amplitude which corresponds to more massive halos.

When observational selection is applied to the GIF simulation, about 3200 galaxies are classified as elliptical galaxies, while about 7500 galaxies are classified as spiral galaxies. The fraction of the early-type galaxies in the simulation is lower than that in the SDSS sample used by M2002 ($\mathrm{E}:\mathrm{S} \approx 1:1$). This may be due to the fact that the definitions used to define early- and late-type galaxies are different in the GIF simulation and in the observations. As mentioned above, galaxies in the GIF simulation are assigned morphological types according to their bulge/disk ratios, while galaxies used in M2002 are classified according to their color, concentration and asymmetry. In Fig.7 we compare the GMCFs of elliptical and spiral galaxies. Early-type galaxies have systematically higher GMCF than late-type galaxies, consistent with the observational results of M2002. The amplitude of GMCF is higher than the observational results. We will discuss this in more detail in the next section.

We have also studied the effect of environment on the GMCF. We count the number of neighbours with projected distances less than $1\,h^{-1}$Mpc from each galaxy and divide galaxies into two high- and low-density subsamples containing equal numbers of objects. This procedure is is similar in spirit, but somewhat simpler than the one adopted by M2002, who defined the local density at the position of a galaxy by the inverse of the area of the polygon obtained from a Voronoi tesselation of the galaxy distribution on the sky.

The mean z'-band luminosities for the high and low-density samples are 3.3 and 2.0 $\times 10^{10}\mathrm{h}^{-2} L_\odot$. The GMCFs for these samples are shown in Fig.8. Galaxies in low-density environments are mainly central galaxies and as a result, their GMCF is fit very well by an NFW halo. Galaxies in high-density environments occur in groups and clusters. Many of them are not central galaxies– this is why the NFW model is a considerably worse fit.

4 THE MASS-LUMINOSITY RELATIONS

One important goal of studying galaxy-galaxy lensing is to derive the relation between luminosities of galaxies and the masses of their host haloes. In this section, we study whether or not the observed GMCF can be used to infer such a mass-luminosity relation.

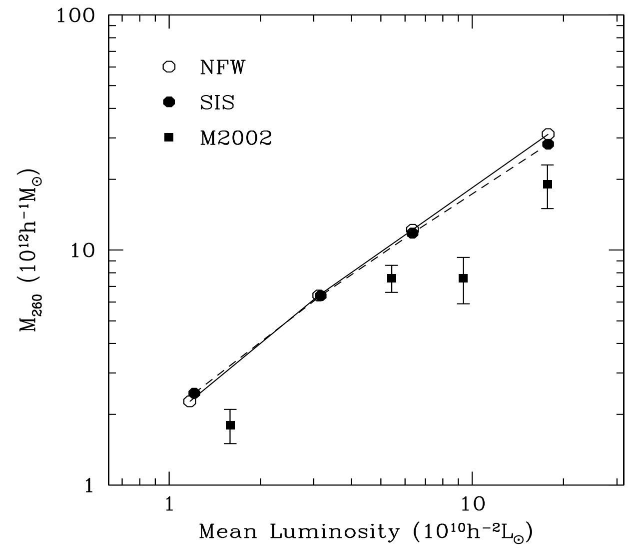

Figure 9. The M_{260}-luminosity relation for galaxies in the GIF simulation. Open circles are based on the fit to the NFW model, while solid circles are based on the fit to the SIS model. The squares with errorbars are the results from M2002.

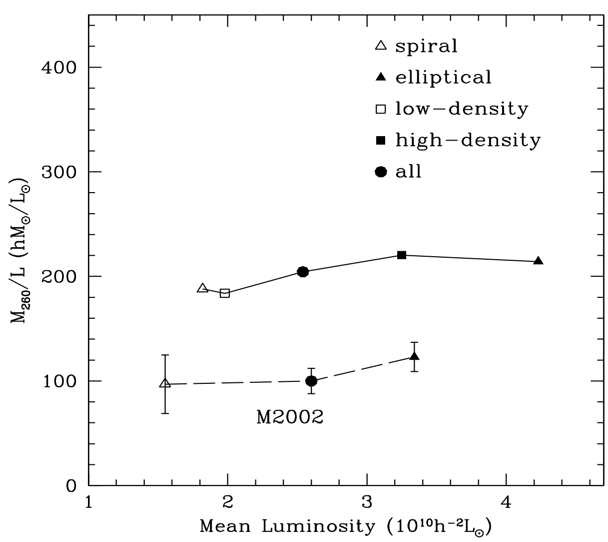

Figure 10. The M_{260}/L ratios for various samples taking into account the observational selections. The mass/light ratios are measured separately for spiral and elliptical galaxies, galaxies in low- and high-density regions, and all galaxies. The results of various simulation samples are connected with a solid line. For comparison, the results of M2002 are shown by symbols connected with a long dashed line.

4.1 The M_{260}-L Relation

In their paper, M2002 attempted to estimate the halo mass within a fixed aperture of radius $R = 260\,h^{-1}$kpc. The reason for this choice is that the GMCF at a much larger radius is likely to be affected by projection effects, and at small radius, the GMCF is difficult to measure observationally (see M2002 for detailed discussion).

In this section we follow the procedure adopted by M2002 and fit the GMCF to a projected singular isothermal sphere (SIS) model to obtain M_{260} for the galaxy samples we have selected out of the simulations:

$$\Delta_+\Sigma(R)_{SIS} = \Sigma(R)_{SIS} = \frac{\sigma_v^2}{2G}\frac{1}{R}, \tag{5}$$

where σ_v is the line-of-sight velocity dispersion. We have also fit the GMCF to a NFW profile, which gives the parameters r_{200} and c (see Subsection 2.2). The aperture mass M_{260} is then the integral of $\Delta\Sigma_+$ within a radius $260\,h^{-1}$kpc.

Fig.9 shows M_{260} as a function of the mean luminosity of galaxies. Both the SIS and NFW models give very similar aperture masses. For comparison, we also display the M_{260}-L relation given by M2002. The predicted trend of mass with luminosity is similar to the observation, but the predicted M_{260} is about a factor of 2 larger than the observed value.

In Fig.10 we show the predicted M_{260}/L ratios for various simulated samples, and compare them with the measurements of M2002. Note that the observational selection is applied to the total sample, rather than to individual samples. This is the reason why the mean luminosities of the morphological samples are somewhat different from the observed values. We find that the M_{260}/L ratios are independent of galaxy luminosity, morphological type and environment, consistent with the observational results. The predicted amplitude of M_{260}/L is about two times the observed value, indicating that the model over-predicts the halo mass (or under-estimates the luminosity).

As shown above, the predicted mass-to-light ratios in the simulations are about two times that of the observed value. Should we take this discrepancy seriously? In the GIF catalogs, model parameters are calibrated to reproduce the observed Tully-Fisher (TF) relation. This calibration depends on how the observed rotation velocities are related to the halo circular velocities and is hence uncertain. Kauffmann et al (1999) have shown that their model underpredict the number density of L_* galaxies by a factor of 2, and so a higher luminosity for a given halo mass may make the model prediction in better agreement with the observed luminosity function around L_*. However, assigning much higher luminosities to dark haloes may lead to too high a luminosity density for the local universe (Kauffmann et al. 1999; see also Yang, Mo & van den Bosch 2002).

4.2 Deriving halo masses from the GMCFs

The relation between the aperture masses M_{260} and the mass of a galaxy's halo is complicated. We have already highlighted one important problem– for "non-central" galaxies in groups, M_{260} will have almost no relation to the mass of the surrounding dark halo. Even if one were to impose an isolation criterion on the sample and select only central galaxies, the relation between M_{260} and M_{halo} is not trivial. For luminous central galaxies, M_{260} only measures the mass in the inner regions of their halos, while for faint central galaxies, M_{260} measures the mass beyond the virial radius of the halo . This is shown in Fig. 11. As one can see, M_{260} is lower than the mean halo mass for bright central galaxies and is higher than the mean halo mass for faint central galaxies. Over a large range of luminosity, the aperture mass M_{260} scales linearly with galaxy luminosity, while the halo mass scales as $L^{1.5}$.

Fig. 12 shows the relation between $M_{\rm halo}$ and M_{260} for

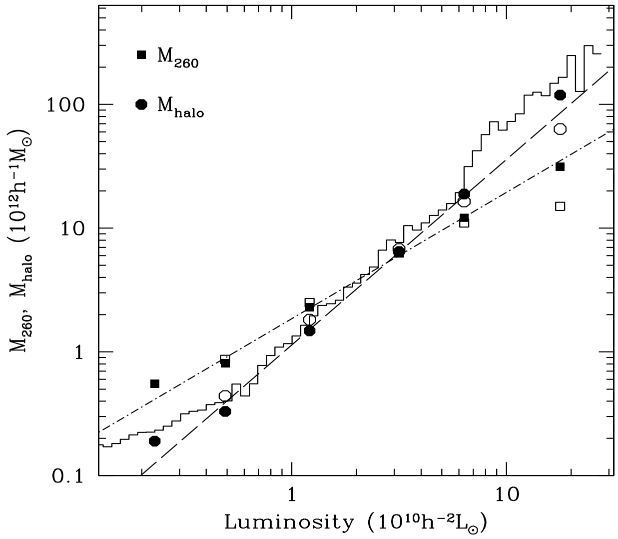

Figure 11. The aperture mass M_{260} (squares) and halo mass $M_{\rm halo}$ (circles) recovered from the GMCFs, together with the mean halo mass directly measured from the simulations (histogram). Solid symbols are for CG samples and open symbols are for low-density samples taking into account of observational selection. The two straight lines show power laws $M \propto L^{1.5}$ and $M \propto L$, respectively. Note that over a large luminosity range, the aperture mass M_{260} in the simulation increases linearly with L, while the halo mass increases roughly as $L^{1.5}$.

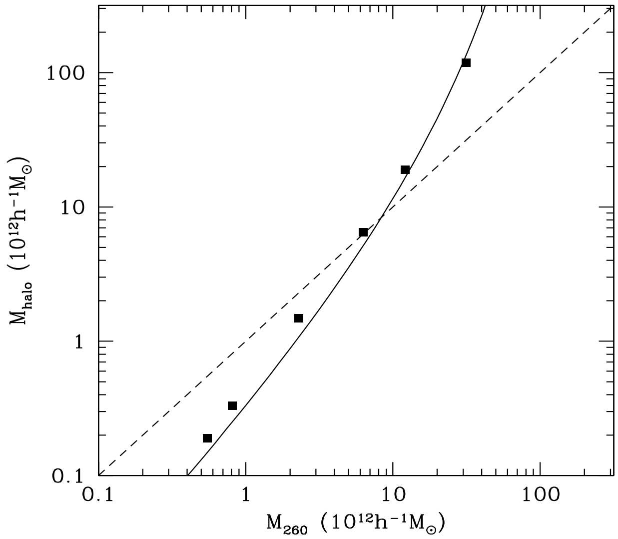

Figure 12. The M_{halo}-M_{260} relation. The solid line is the prediction of a simple model discussed in the text. The squares are inferred from the GMCF for CG samples.

central galaxies in the simulation. Once again we see that $M_{\rm halo}$ and M_{260} are tightly correlated, but the relation is not linear. For haloes more massive than $10^{13}h^{-1}{\rm M}_\odot$, $M_{\rm halo}$ is larger than M_{260}, while for less massive haloes, $M_{\rm halo}$ is smaller than M_{260}. This relation can also be obtained using a simple analytical model. From numerical simulations, it is known that the concentration of a halo c is correlated with M. We use the $c-M$ relation obtained by Bullock et al. (2002):

$$c(M) \approx 9\left(\frac{M}{M_*}\right)^{-0.13}, \tag{6}$$

where M_* is the characteristic non-linear mass scale at which the *rms* of the linear density field is equal to the critical overdensity for spherical collapse, $\sigma(M_*) = \delta_c \sim 1.69$. The definition of the halo mass M is somewhat different from ours, but this relation changes only a little. With this model, we can predict $M_{\rm halo}$ as a function of M_{260}. The solid curve in Fig. 12 shows this prediction.

We now ask how one can derive halo masses from the full GMCF. One possibility is to use the results of the NFW fit to the GMCF to obtain an average 'halo mass' (denoted by $M_{\rm halo}$) for a set of lens galaxies that have no close neighbours of comparable brightness and are thus likely to be "central" objects. In Fig. 11 we plot the mass recovered this way as a function of galaxy luminosity for the central galaxies in our simulation (solid dots). A comparison with the mean halo mass measured directly from the simulation shows that the agreement is very good over a large range of halo masses. Thus, for central galaxies, this method works well in recovering the mean halo mass. The open circles in Fig. 11 show the recovered halo masses for the sample of galaxies in low-density environments defined in section 3.3. The results are very close to that for central galaxies, except at the very bright end where the halo mass is lower because bright galaxies in massive, rich clusters are missing. Thus, it is also possible to obtain the halo mass of galaxies by using the GMCFs of galaxies in low-density environments. In the next subsection we will apply this method to the data of M2002 to derive halo masses for the observed galaxies as a function of luminosity.

The second method for deriving halo masses is to make use of the relation between $M_{\rm halo}$ and M_{260} obtained from simulations (Fig. 12). This will be described in more detail in the next section.

4.3 Halo masses of the observed galaxies

We now apply our two methods of estimating halo masses to the actual observational data. Fig.13 shows the results of fitting a NFW profile to the GMCFs of M2002 (their Fig. 15). As in M2002, we have used only data points at projected radii smaller than $260\,h^{-1}$kpc. In order to obtain stable results, we have assumed that the concentration c depends on halo mass as in equation (6). The open circles in Fig.14 show the halo mass obtained in this way as a function of galaxy luminosity. The errorbars on the derived masses assume that the observed errors on the GMCF at different radii are independent and are Gaussian distributed. Since the observed errors at different radii are actually correlated, the real errorbars on $M_{\rm halo}$ should be smaller than those shown in the figure.

The other way to derive $M_{\rm halo}$ is to convert the aperture mass M_{260} into a halo mass using the relation shown in Fig.12. These results are shown as solid squares in Fig.14, and the errorbars are obtained directly from the errorbars on the observed M_{260}. The halo masses derived from these two methods are very similar.

As one can see, the halo mass increases with luminosity roughly as a power law. A simple linear regression of all the data points gives

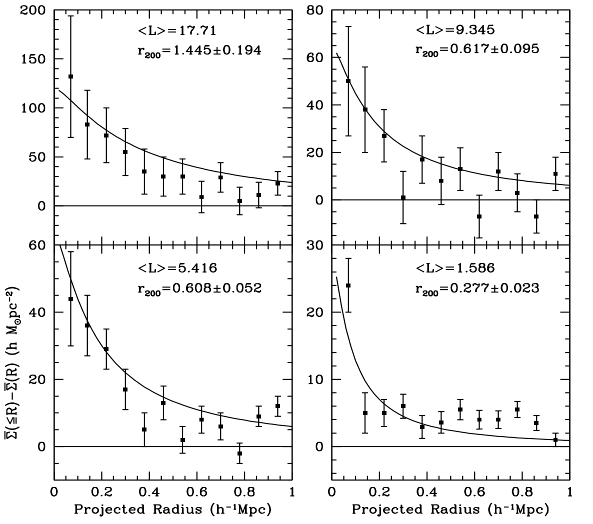

Figure 13. The NFW fits to the observed z' band GMCF data in Fig. 15 of M2002. Here we assume that the concentration c depends on the halo mass as Eq. (6), and use r_{200} as the only free parameter. The fits only extend over radii smaller than $260\,h^{-1}$kpc, as in M2002.

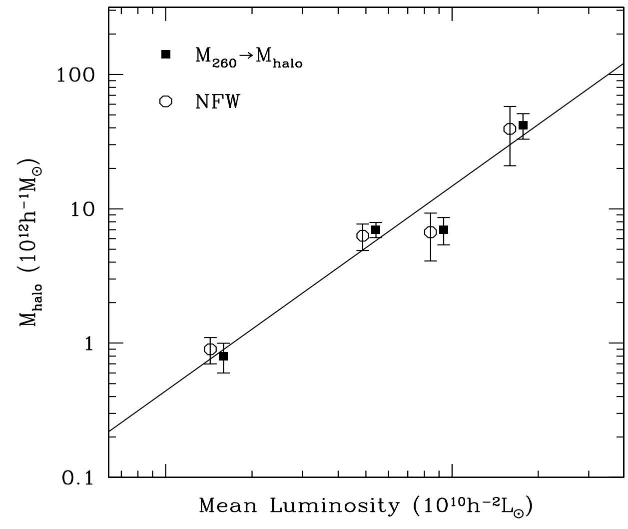

Figure 14. The derived halo masses M_{halo} as a function of luminosity. The squares show M_{halo} estimated using the relation shown in Fig.12. The circles are the halo masses obtained from the fits in Fig. 16. Errorbars are estimated using 1-σ variances of the data points. To avoid confusion, the results of the NFW fit are shifted to the left. The solid line is a power law fit of the data points shown.

$$M_{\rm halo} \approx 2.0 \times 10^{12} h^{-1} {\rm M}_\odot \left(\frac{L}{L_*}\right)^{1.5}, \tag{7}$$

where $L_* \approx 2.56 \times 10^{10} h^{-2} {\rm L}_\odot$ is the characteristic luminosity in the z'-band (Blanton et al. 2001). This scaling is similar to that obtained from the GIF simulation (see Fig. 11). In terms of mass-to-light ratio, we can write

$$\frac{M_{\rm halo}}{L} \approx 75h \left(\frac{L}{L_*}\right)^{0.5} \frac{{\rm M}_\odot}{{\rm L}_\odot}. \tag{8}$$

This mass-to-light ratio is about two times smaller than the simulation results. The origin of this discrepancy has already been discussed in Subsection 4.1.

The power index 1.5 we obtain for the $M_{\rm halo}$–L relation is similar to that derived by Guzik & Seljak (2002) using an analytic model of the galaxy distribution in dark haloes. However, our value of the mass-to-light ratio for L_* galaxies is about two times larger than theirs. One possible reason for this discrepancy is that Guzik and Seljak assume that galaxies in groups and clusters have the same halo masses as isolated galaxies of the same luminosity. If galaxy halos in groups are tidally truncated, their assumption will cause the halo masses of isolated galaxies to be underestimated. Current high-resolution N-body simulations (e.g. Klypin et al. 1999; Moore et al. 1999; Springel et al. 2001) show that subhalos of dark matter in galaxy systems have radii typically much smaller than 200 kpc, and so their contribution to the lensing signals on the scales we are concerned here should not be important.

Since the ratio M_{260}/L does not depend on morphological type, we may apply our method to spirals to check whether their halo masses are consistent with those derived from the Tully-Fisher relation (e.g. Hudson et al. 1998; Smith et al. 2001; Wilson et al. 2001; Seljak 2002).

In the I-band, the observation of Giovanelli et al. (1997) gives

$$L_I \approx 1.0 \times 10^{10} \left(\frac{V_{\rm obs}}{150\,{\rm km\,s^{-1}}}\right)^{3.1} h^{-2} {\rm L}_{\odot I}, \tag{9}$$

where $V_{\rm obs}$ is an observational measure of the rotation velocity, usually taken as the maximum rotation velocity. The typical $z' - I$ colour of a spiral galaxy is similar to that of the Sun, so its luminosity in solar units will have the same value in different bands. Thus, for an L_* galaxy with z'-band luminosity $2.56 \times 10^{10} h^{-2} {\rm L}_\odot$, the Tully-Fisher relation implies $V_{\rm obs} \approx 205\,{\rm km\,s^{-1}}$. If we include an internal extinction of about 0.3^m (see Verheijen 2001) this will increase $V_{\rm obs}$ to about $225\,{\rm km\,s^{-1}}$. The halo mass for an L_* galaxies obtained from the Tully-Fisher relation is thus

$$M_{{\rm halo},*} \sim 4.8 \times 10^{12} h^{-1} \left(\frac{V_c}{V_{\rm obs}}\right)^3 {\rm M}_\odot, \tag{10}$$

where V_c is the circular velocity of the halo. We have assumed $\Omega_0 = 0.3$, and defined the halo radius such that the mean density within it is 200 times the mean density of the Universe. Comparing this with the lensing result given in equation (7), we see we require $V_{\rm obs}/V_c \sim 1.34$. This ratio is consistent with the predictions of disk formation models (e.g. Mo, Mao & White 1998; Mo & Mao 2000). The $V_{\rm obs}/V_c$ ratio obtained here is lower than that obtained by Seljak (2002) based on the mass determination published in Guzik & Seljak (2002). This is because our estimated halo mass is higher than theirs.

5 DISCUSSION AND SUMMARY

In this paper we have used galaxy catalogues constructed from a high-resolution numerical simulation to investigate the properties of the projected galaxy-mass correlation function (GMCF) measured from weak galaxy-galaxy lensing observations. A comparison between the predicted GMCFs with those obtained recently by McKay et al. (2002) from the Sloan Digital Sky Survey (SDSS) data shows that the observed dependence of the GMCF on galaxy luminosity, morphological type and environment is well reproduced in the model. In the simulations, the ratio between the aperture mass within a radius of $260\,h^{-1}$kpc and lens galaxy luminosity is independent of galaxy luminosity, type and environment. The value of M_{260}/L is approximately equal to the ratio between the halo mass (defined to be the mass within the halo virial radius) and luminosity for L_* galaxies. M_{260} overestimates the halo mass for lens galaxies with $L \ll L_*$ and underestimates the halo mass for $L \gg L_*$.

Using the simulations, we show that halo masses can be recovered by fitting the full GMCF with realistic halo density profiles. If we apply this method to the observational data, we find that the halo mass scales with galaxy luminosity as $M_{\rm halo} \propto L^{1.5}$. The mean halo mass we derive for an L_* spiral galaxy is consistent with that inferred from the observed Tully-Fisher relation.

We find that the behavior of the GMCF can be significantly affected by satellite galaxies in high-density environments. The observed GMCF can only be used to probe the properties of individual galaxy haloes if galaxy samples are limited to central galaxies. We have demonstrated that an effective way of doing this is to select bright and relatively isolated galaxies. In the future when lensing signal can also be detected for galaxies fainter than L_* (many of which are expected to be satellite galaxies), detailed modelling of the galaxy distribution in dark halos will be required to compare models and observations.

Our results suggest that the GMCF obtained from galaxy-galaxy lensing can provide important constraints on galaxy formation models. With the completion of the SDSS, such constraints will become an integral part of our understanding of galaxy formation.

ACKNOWLEDGEMENT

We thank Simon White for useful suggestions and the GIF group for the public release of their N-body simulation data. XHY thanks the CAS-MPG exchange program for support.

APPENDIX A: THE PROJECTION OF NFW PROFILE

The properties of the projected NFW profile can be found in, *e.g.*, Bartelmann (1996). The surface mass density can be expressed as a function of a dimensionless radius $x \equiv R/r_s$:

$$\Sigma(x) = A\ f(x) \tag{A1}$$

where

$$\begin{aligned} f(x<1) &= \frac{1}{x^2-1}\left(1-\frac{\ln\frac{1+\sqrt{1-x^2}}{x}}{\sqrt{1-x^2}}\right) \\ f(x=1) &= \frac{1}{3} \\ f(x>1) &= \frac{1}{x^2-1}\left(1-\frac{\operatorname{atan}\sqrt{x^2-1}}{\sqrt{x^2-1}}\right) \end{aligned} \tag{A2}$$

and

$$A = 2\ r_s\ \bar{\delta}\ \bar{\rho_c}\ . \tag{A3}$$

The mean surface mass density within radius x is:

$$\Sigma(\le x) = A\ g(x) \tag{A4}$$

where

$$\begin{aligned} g(x<1) &= \frac{2}{x^2}\left(\ln\frac{x}{2}+\frac{\ln\frac{1+\sqrt{1-x^2}}{x}}{\sqrt{1-x^2}}\right) \\ g(x=1) &= 2+2\ln\frac{1}{2} \\ g(x>1) &= \frac{2}{x^2}\left(\ln\frac{x}{2}+\frac{\operatorname{atan}\sqrt{x^2-1}}{\sqrt{x^2-1}}\right) \end{aligned} \tag{A5}$$

The mass density contrast is simply

$$\Delta\Sigma_+(x) = A\ [g(x)\ -\ f(x)]\,. \tag{A6}$$

APPENDIX B: CONTRIBUTION BY SATELLITE GALAXIES

If the lens galaxy is not located at the center of its halo, the average surface mass density and the GMCF will depend on an extra parameter R_c, the distance between the galaxy and the center of the halo. The average surface mass density in this case is

$$\Sigma'(r) = \frac{1}{2\pi}\int_0^{2\pi} \Sigma(r')\mathrm{d}\theta \tag{B1}$$

where $\Sigma(r')$ is the NFW surface mass density and $r' = \sqrt{R_c^2 + r^2 + 2R_c r\cos\theta}$.

In Fig. B1 we show the surface mass density (upper panel) and the density contrast (lower panel) as a function of radius R for various choices of R_c. The parameters are set to be $r_{200} = 1.2\,h^{-1}$Mpc, $c = 6.0$, and R_c changes from 0 to $0.4\,h^{-1}$Mpc. The figure shows that the surface mass density has a peak near R_c, while the density contrast reaches a minimum near R_c and then increases rapidly with increasing radius. Clearly, the behavior of the GMCF for satellite galaxy is very different from that for central galaxy (corresponding to $R_c = 0$). The complex behavior of the GMCF of satellite galaxies complicates the interpretation of the observed GMCF, and so it is important to separate central and satellite galaxies in the galaxy-galaxy lensing study. As we have demonstrated above, selections of central galaxies can be made quite effectively by using bright and relatively isolated galaxies.

REFERENCES

Bartelmann M., 1996, A&A, 313, 697
Blanton, M.R., Dalcanton, J., Eisenstein, D., et al., 2001, AJ, 121, 2358B
Bullock J.S., Kolatt T.S., Sigad Y., Somerville R.S., Klypin A.A., Primack J.R., Dekel A., 2001, MNRAS, 321, 559
Diaferio A., Kauffmann G., Colberg J. M., & White S. D. M. 1999, MNRAS, 307, 537
Diaferio A., Kauffmann G., Balogh M.L., White S.D.M., Schade D., Ellingson E., 2001, MNRAS, 323, 999
Fischer, P., McKay, T. A., Sheldon, E., et al., 2000, AJ, 120, 1198F

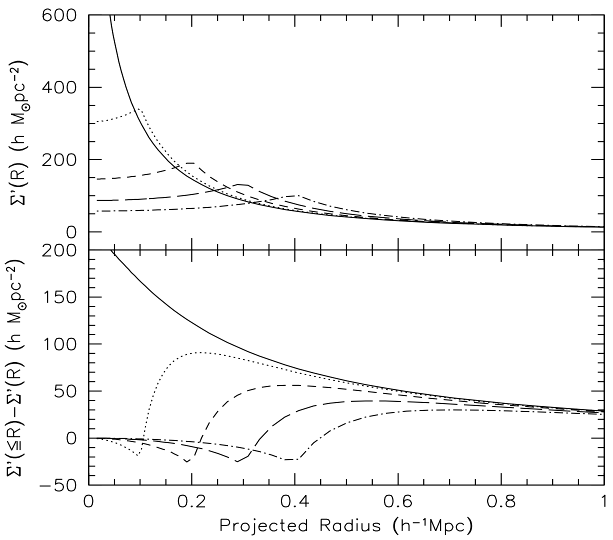

Figure B1. The surface density (upper panel) and density contrast (lower panel) around satellite galaxies as a function of radius R. The results are shown for a single NFW halo with $r_{200} = 1.2\,h^{-1}$Mpc and $c = 6.0$. Different curves correspond to different distances between the satellite and the halo center: $R_c = 0$ (solid); 0.1 (dotted); 0.2 (dashed); 0.3 (long dashed); 0.4 (dot-dashed) (all in units of h^{-1}Mpc).

Giovanelli, R.M., Haynes, M.P., Da Costa, L.N., Freudling, W., Salzer, J.J. & Wegner, G., 1997, ApJ, 477, L1

Guzik, J. & Seljak, U. 2002, astro-ph/0201448

Hudson M.J., Gwyn S.D.J., Dahle H. Kaiser N., 1998, ApJ, 503, 531

Jenkins, A., Frenk, C. S., Pearce, F. R., et al., 1998, ApJ, 499, 20

Kauffmann, G., Colberg, J. M., Diaferio, A., & White, S. D. M. 1999a, MNRAS, 303, 188

Kauffmann, G., Colberg, J. M., Diaferio, A., & White, S. D. M. 1999b, MNRAS, 307, 529

Klypin A., Gottloeber S., Kravtsov A.V., Khokhlov A.M., 1999, ApJ, 516, 530

Mckay, T. A., Sheldon, E. D., Racusin, J., et al., 2002, submitted to ApJ, also astrp-ph/0108013

Mo, H.J., Mao, S., 2000, MNRAS, 318, 163

Mo, H.J., Mao, S., White 1998, MNRAS, 295, 319

Moore B., Ghigna S., Governato F., Lake G., Quinn T., Stadel J., Tozzi P., 1999, ApJ, 524, L19

Navarro, J. F., Frenk, C. S., & White, S. D. M. 1997, ApJ, 490, 493

Schneider, P., Ehlers, J, & Falco, E.E., 1999, Gravitational lenses, A&A Library. Springer Verlag: Berlin

Seljak, U. 2002, astro-ph/0201450

Smith D.R., Bernstein G.M., Fischer P., Jarvis M., 2001, ApJ, 551, 643

Springel V., White S.D.M., Tormen G., Kauffmann G., 2001, MNRAS, 328, 726

Verheijen M.A.W., 2001, ApJ, 563, 694

Wilson G., Kaiser N., Luppino G.A., & Cowie L.L., 2001, ApJ, 555, 572

Yang X.H., Mo H.J., & van den Bosch F.C., 2002, to be submitted